Short communication

A TEM study of cycled nano-crystalline HT-LiCoO$_2$ cathodes for rechargeable lithium batteries

Sun Hee Choi[a], Joosun Kim[a], Young Soo Yoon[b,*]

[a] *Nano-Materials Research Center, Korea Institute of Science and Technology, P.O. Box 131, Cheongryang, Seoul 130-650, Republic of Korea*
[b] *Department of Advanced Fusion Technology, (Center for Emerging Wireless Power Transmission Technology),
Konkuk University, Seoul 143-701, Republic of Korea*

Abstract

LiCoO$_2$ has α-NaFeO$_2$ structure type and it has been reported that layered cation ordering is preserved during repeated insertion and removal of Li$^+$. We have observed, at a nano-particle scale, cation disorder induced in LiCoO$_2$ after prolonged cycling. LiCoO$_2$ cathode powders with nano-grain sized of 70–300 nm were synthesized by a mechano-chemical method. Transmission electron microscopy study of LiCoO$_2$ showed that the initial O$_3$ crystal structure partially transformed to a cubic spinel phase. This spinel phase formation may be responsible for capacity degradation after prolonged cycling of LiCoO$_2$-based rechargeable lithium batteries. Cycle life of small size (70 nm) LiCoO$_2$ powder until 200 cycles is better than that of large size (300 nm) LiCoO$_2$ powder due to shorter diffusion distance.
© 2004 Elsevier B.V. All rights reserved.

Keywords: Transmission electron microscopy; LiCoO$_2$; Disordered phase transformation; Spinel; Capacity fade

1. Introduction

LiCoO$_2$ heat-treated above 700 °C (HT-LiCoO$_2$) has a high cycle life compared to other cathode materials, such as LiNiO$_2$ and LiMn$_2$O$_4$. The structure of LiCoO$_2$ is rhombohedral (R3m space group) with lattice parameters $a = 2.816$ Å and $c = 14.051$ Å in a hexagonal setting. The lattice is formed by oxygen atoms in ABC stacking with alternating layers of Li and Co ions in octahedral interstitial sites between the oxygen planes [1–4]. Recently, an useful method for the preparation of nano-crystalline individual oxides has been found during studies of mechano-chemical solid state exchange reactions [5,6]. Mixing the reaction products with inert thermostable salt prevents particle coarsening during further heat treatment of the reaction mixture. Combination of salt encapsulation with an earlier proposed powder engineering technique [7,8] ensures fine particle size control of LiCoO$_2$ powders obtained by wet chemical methods [9].

During delithiation, Li$_x$CoO$_2$ experiences a sequence of phase transformations involving Li ordering within its octahedral layers, accompanied by changes in crystal symmetry, first to the monoclinic and then to the hexagonal phase. There have been many studies on how the crystal structure changes over one charge–discharge cycle [10–12]. The typical reversible limit of delithiation for Li$_x$CoO$_2$ in commercial batteries is $x \sim 0.5$ [2], corresponding to a charge capacity of $\sim$140 mA h/g. This has been mostly attributed to mechanical failure associated with the large change in the c-axis dimension, rather than any changes in cation ordering. There have been few studies, however, on how the crystal structure changes after prolonged cycling [13]. In the present work, we have used transmission electron microscopy (TEM) to study microstructural changes of nano-crystalline LiCoO$_2$ after prolonged cycling.

2. Details of experiment

An aqueous solution of Li and Co acetates (Li/Co = 1.1) was frozen by spraying on liquid nitrogen followed by freeze drying for 2 days at $P = 5 \times 10^{-2}$ mBar (Alpha 2–4, Christ). A part of the freeze-dried product was mixed with K$_2$SO$_4$ (1:10) and subjected to planetary milling (Pulverisette-5, Fritsch) in ZrO$_2$ media at 600 rpm for 24 h (ball to powder
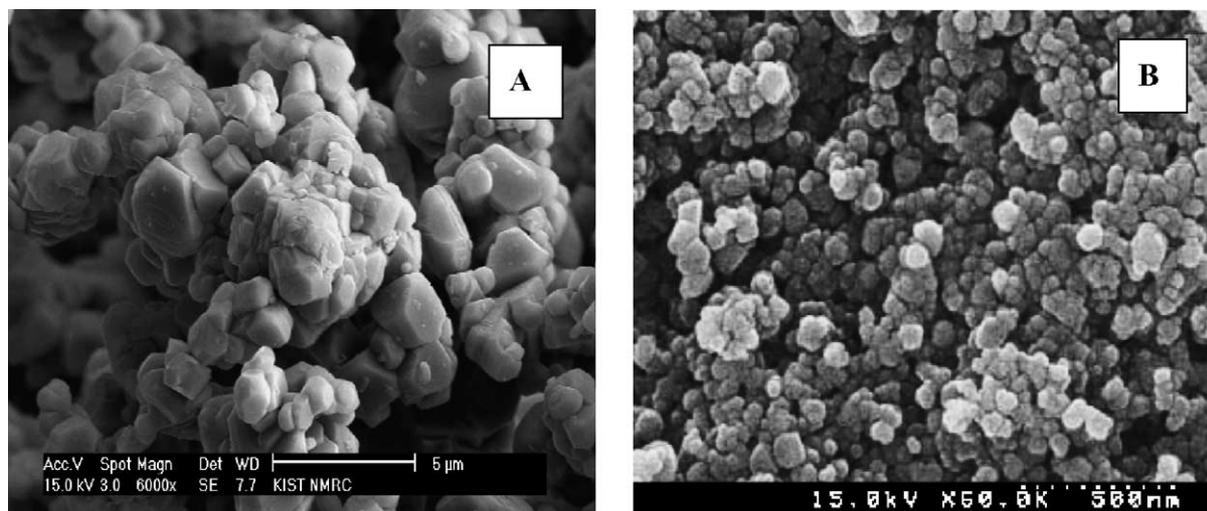
Fig. 1. SEM micrographs of LiCoO$_2$ powders (A) Seimi Co. and (B) planetary processing with K$_2$SO$_4$.

mass ratio of 10:1). Thermal decomposition of a precursor and a precursor mixture with K$_2$SO$_4$ was performed in air first at 400 °C for 10 h, then at 800 °C for 12 h. The thermally processed mixture was washed by distilled water several times for elimination of SO$_4{}^{2-}$ ions; LiCoO$_2$ residue was separated by centrifuging.

Obtained LiCoO$_2$ powders have been studied by XRD (Geigerflex, Rigaku, 2°/min, Cu Kα), scanning electron microscopy (SEM, Philips ESEM) and TEM (Philips CM-30,

$U = 200$ kV). Commercial LiCoO$_2$ powder, supplied by Seimi Co. was used for comparison.

Electrochemical characterizations were performed using a CR2032 coin-type cell with the following parameters: cut-off voltage 3.2–4.2 V and $I = 0.5$ mA at room temperature. The cathode was fabricated with 20 mg of accurately weighed active material and 12 mg of conductive binder (8 mg of teflonized acetylene black (TAB) and 4 mg graphite). The cathode was pressed on 200 mm^2 stainless
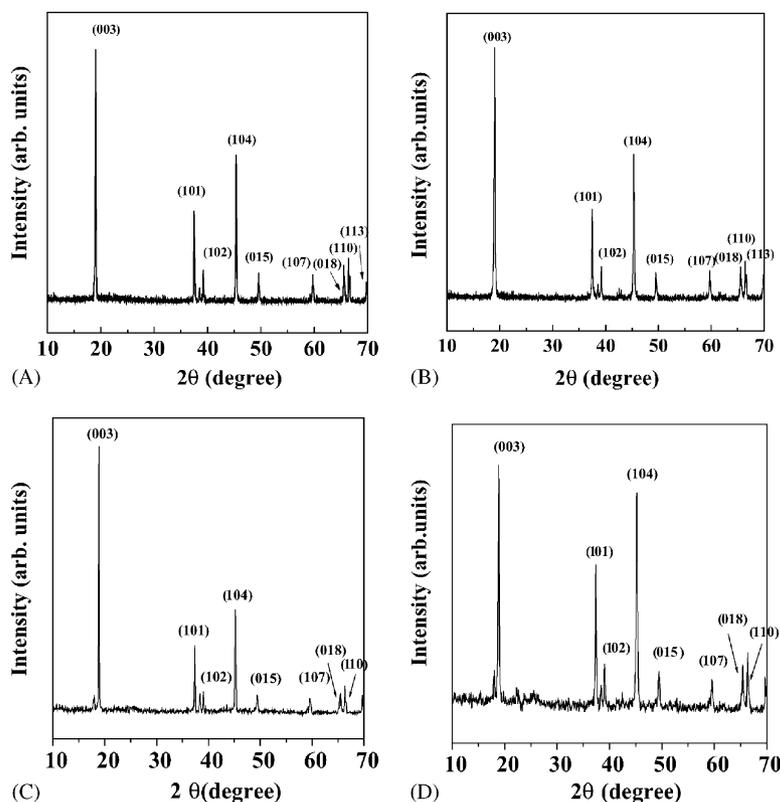

Fig. 2. XRD patterns of (A) coarse-grained Seimi Co., (B) nano-crystalline LiCoO$_2$ powders, (C) cycled coarse-grained Seimi Co. and (D) cycled nano-crystalline LiCoO$_2$ powders.

steel mesh, which was used as the current collector, under a pressure of $300 \, kg/cm^2$ and subsequently dried at $180 \, °C$ for 24 h in a vacuum oven. The test cell was made of cathode and a lithium metal as an anode separated by a porous polypropylene film (Celgard 3401). A mixture of 1 M $LiPF_6$-ethylene carbonate (EC)/dimethyl carbonate (DMC) (1:2 by vol., Merck) was used as the electrolyte.

We focused on a cell that was electrochemically cycled 10 times and the cycled material left in the discharged (lithiated) state. The cell was disassembled and cycled $LiCoO_2$ powders were obtained by washing in *n*-methyl-pyrrolidinone (NMP) to dissolve the binder. Specimens for TEM analysis were prepared from a suspension of $LiCoO_2$ powder in methanol. A droplet was placed on a carbon film supported by a copper grid.

3. Results and discussion

SEM analysis of the $LiCoO_2$ powders, obtained by matrix isolation of precursor particles by K_2SO_4, confirmed the efficiency of this method in terms of grain coarsening prevention. Commercial Seimi Co. powder (powder A) formed micron-sized crystallites (Fig. 1A), while K_2SO_4-processed powder (powder B) was characterized by a grain size distribution in a range of 30–70 nm (Fig. 1B).

XRD analysis of micron-sized (powder A) and nano-crystalline powders (powder B) revealed the formation of single phase hexagonal HT-$LiCoO_2$ in both cases (Fig. 2A and B). Processing of $LiCoO_2$ powders at $800 \, °C$ in contact with K_2SO_4 was not accompanied by formation of secondary phases or by significant displacement of the main reflections displayed in the formation of solid solutions. Sharp and well-resolved reflections of both patterns were observed at perfect crystallographic ordering. The uncharacteristic $(0\,0\,3)/(1\,0\,4)$ peak ratio for the nano-crystalline powder can be related to anomalies of element distribution within the Co sublattice [14]. Comparing the XRD of uncycled (Fig. 2A and B) and cycled cathodes (Fig. 2C and D), we confirmed that the characteristic peak positions of the $LiCoO_2$ phase remained unchanged. Extraneous peaks in the cycled cathodes arose from the binder. The relative intensities of the peaks changed; however, this may be due to varying levels of preferential orientation introduced during preparation of the XRD samples.

The electron diffraction pattern of powder A, recorded along the $[0\,0\,0\,1]$ zone axis, was also typical for well-ordered $LiCoO_2$ with hexagonal structure (Fig. 3A). The major spots corresponded to the $\{1\,1\,\bar{2}\,0\}$ reflections. On the other hand, SAED pattern of the small particles in powder B (Fig. 3B) partially contained cubic spinel phase. These patterns were attributed to the formation of a spinel structure due to cation disorder in the hexagonal lattice of $LiCoO_2$. In the case of powder B, partial cubic spinel phase affected the electrochemical characteristics of the $LiCoO_2$ cathode. This result is discussed hereafter.
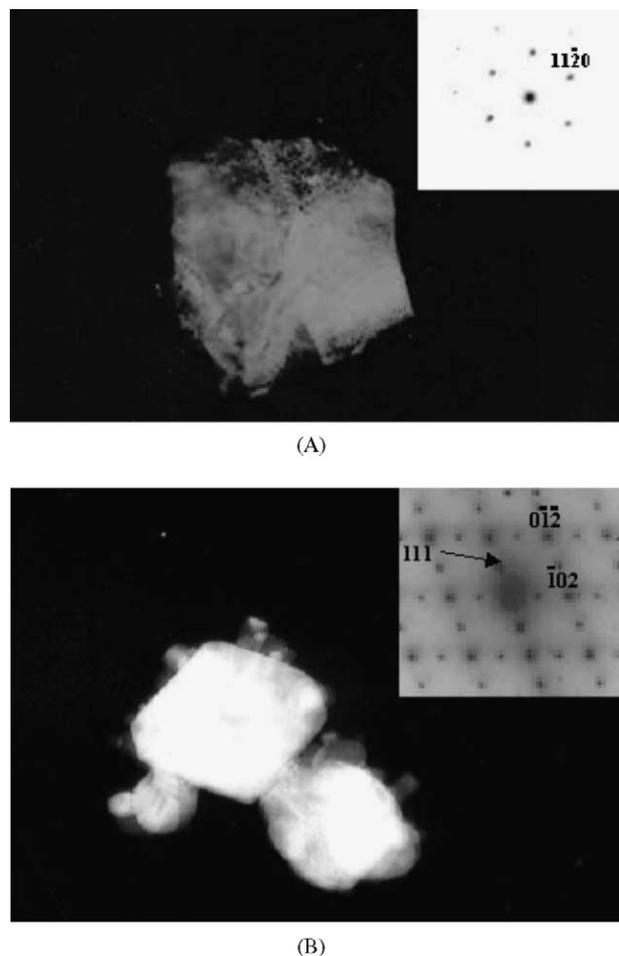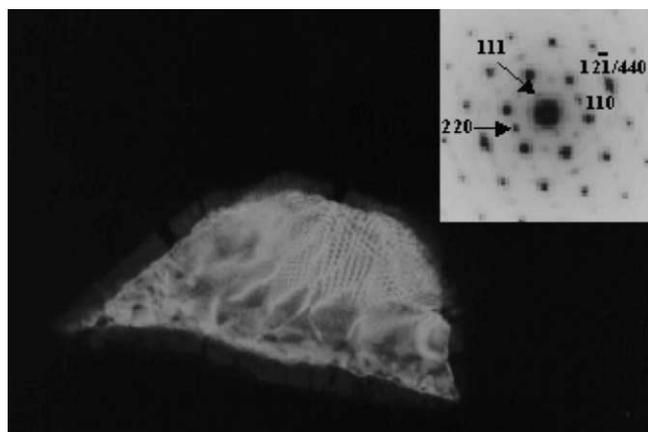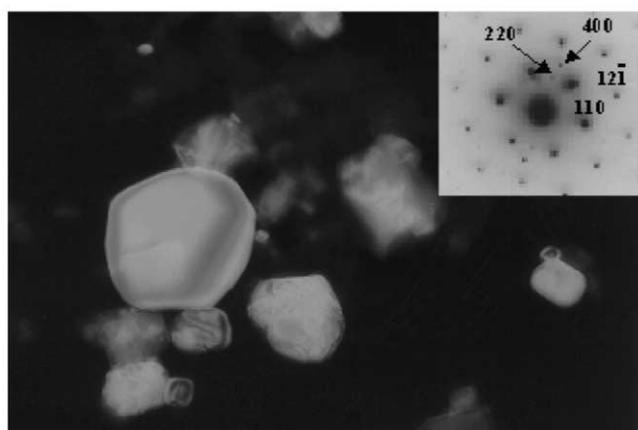

(A)

(B)

Fig. 3. Bright field TEM and selected area electron diffraction (SAED) patterns of coarse-grained Seimi Co. ($[0\,0\,0\,1]$ zone axis) (A) and nano-crystalline ($[2\,\bar{2}\,1]$ zone axis) (B) $LiCoO_2$ powders.

After electrochemical cycling some particles displayed a variety of contrast features including strain contours and other extended defects as compared to uncycled powders. Stresses can arise from lattice expansion and contraction, because upon delithiation Li_xCoO_2 exhibits a *c*-axis expansion of upto 1.8% at $x \cong 0.5$, followed by a *c*-axis contraction of upto -1.8% at $x \cong 0.2$ [11]. Microstructural changes in $LiCoO_2$ were observed after 10 cycles. The diffraction pattern of Fig. 4, recorded along the $[\bar{1}\,1\,1]$ zone axis, shows weak new diffraction spots that lie halfway between the fundamental $\langle 1\,2\,\bar{1} \rangle$ diffraction spots ($\{1\,1\,\bar{2}\,0\}$ reflections at $[0\,0\,0\,1]$ zone axis) observed in the uncycled material. This indicates a change in the crystal structure. These diffractions were $\{2\,2\,0\}$ superlattice diffractions, characteristic of the cubic spinel phase. Cubic spinel $LiCoO_2$ with both Li and Co sitting on octahedral 16c and 16d sites displayed a $\{2\,2\,0\}$ peak. We confirmed from diffraction patterns that the initial O_3 crystal structure partially transformed to a cubic spinel phase after electrochemical cycling.

In addition, other new reflections appeared in the cycled powders of both powder A and B. These reflections, in-

(A)

(B)

Fig. 4. Bright field TEM and selected area electron diffraction (SAED) patterns of cycled coarse-grained Seimi Co. ([$\bar{1}$ 1 1] zone axis) (A) and cycled nano-crystalline ([$\bar{1}$ 1 1] zone axis); (B) LiCoO$_2$ powders.

dexed as $\{1\,1\,0\}$ ($\{1\,0\,\bar{1}\,0\}$ reflections at $[0\,0\,0\,1]$ zone axis), are forbidden reflections for HT-LiCoO$_2$. We occasionally observed these reflections in uncycled powders calcined at lower temperatures as well. The $\{1\,1\,0\}$ reflections remain extinct as long as the cation site symmetry is unchanged and all cations within each layer have identical properties. Instead, when Li/Co substitutional disorder occurs, the cation sites are chemically inhomogeneous and the cation site symmetry is reduced. Therefore, these crystallographic defects can cause $\{1\,1\,0\}$ reflections (Fig. 4).

Fig. 5 shows the cycle performance of coarse-grained (powder A) and nano-crystalline (powder B) LiCoO$_2$ cathode. The initial discharge capacity of powder B is smaller than that of powder A. The smaller discharge capacity is due to the partial cubic spinel phase in powder B (Fig. 3B). Since the cubic spinel phase is less electrochemically active, its formation could be a source of the capacity loss. However, the cycle life of powder B until 200 cycles is better than that of powder A. The superior cycle performance of powder B is due to the smaller particle size. Smaller particle size ensures shorter mean length of Li diffusion pathways from its posi-
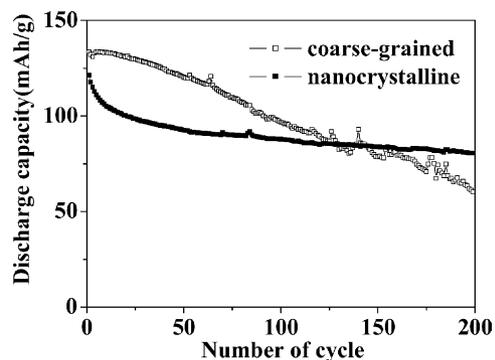

Fig. 5. Cycle performance for coarse-grained Seimi Co. and nano-crystalline LiCoO$_2$ cathodes.

tion in the LiCoO$_2$ lattice to the cathode–electrolyte interface. Also, diffusion through the grain boundary of powder B is larger than that of powder A. Shorter diffusion distances promote faster and more uniform Li intercalation into LiCoO$_2$ crystallites during the discharge process compared to powder A, thus increasing the effective capacity values.

4. Conclusions

We have observed, at a particle scale, cation disorder induced in LiCoO$_2$ after prolonged cycling. Transmission electron microscopy study of LiCoO$_2$ showed that the initial O$_3$ crystal structure partially transformed to a cubic spinel phase. This spinel phase formation may be responsible for capacity degradation after prolonged cycling of LiCoO$_2$-based rechargeable lithium batteries.

The initial discharge capacity of nano-crystalline LiCoO$_2$ (powder B) is smaller than that of a coarse-grained LiCoO$_2$ (powder A) cathode due to the partial cubic spinel phase in nano-crystalline LiCoO$_2$. However, the cycle life of powder B until 200 cycles is better than that of powder A, due to smaller particle size.

Acknowledgements

References

[1] W.D. Johnston, R.R. Heikes, D. Sestrich, J. Phys. Chem. Solids 7 (1958) 1.
[2] K. Mizushima, P.C. Jones, P.J. Wiseman, J.B. Goodenough, Mater. Res. Bull. 15 (1980) 783.
[3] H.J. Orman, P.J. Wiseman, Acta Crystallogr. C40 (1984) 12.
[4] T.A. Hewston, B.L. Chamberland, J. Phys. Chem. Solids 48 (1987) 97.

[5] T. Tsuzuki, E. Pirault, P.G. McCormick, Nanostruct. Mater. 11 (1999) 125.

[6] L.M. Cukrov, T. Tsuzuki, P.G. McCormick, Scripta Mater. 44 (2001) 1787.

[7] V.V. Ischenko, O.A. Shlyakhtin, N.N. Oleinikov, et al., Physica C 282–287 (1997) 855.

[8] Yu. D. Tretyakov, N.N. Oleinikov, O.A. Shlyakhtin, Cryochemical Technology of Advanced Materials, Chapman & Hall, London, 1997, p. 195.

[9] O.A. Shlyakhtin, Y.S. Yoon, Y.-J. Oh, J. Eur. Ceram. Soc. 23 (2003) 1893.

[10] J.N. Reimers, J.R. Dahn, J. Electrochem. Soc. 139 (1992) 2091.

[11] G.G. Amatucci, J.M. Tarascon, L.C. Klein, J. Electrochem. Soc. 143 (1996) 1114.

[12] T. Ohzuku, A. Ueda, J. Electrochem. Soc. 141 (1994) 2972.

[13] J. Li, E. Murphy, P.A. Kohl, J. Power Sour. 102 (2001) 294.

[14] K. Kanamura, A. Goto, R.Y. Ho, et al., Electrochem. Solid State Lett. 3 (2000) 256.